Electrochimica Acta 55 (2010) 1880–1887

Contents lists available at ScienceDirect

Electrochimica Acta

journal homepage: www.elsevier.com/locate/electacta

Electrochemical behavior of Mg and some Mg alloys in aqueous solutions of different pH

Waheed A. Badawy[a,*], Nadia H. Hilal[b], Mohmmed El-Rabiee[b], H. Nady[b]

[a] Chemistry Department, Faculty of Science, University of Cairo, 12 613 Giza, Egypt
[b] Chemistry Department, Faculty of Science, Fayoum University, Fayoum, Egypt

ARTICLE INFO

Article history:
Received 29 July 2009
Received in revised form 30 October 2009
Accepted 30 October 2009
Available online 10 November 2009

Keywords:
Alloys
Corrosion
Impedance
Magnesium
Polarization

ABSTRACT

The electrochemical behavior of Mg, Mg–Al–Zn and Mg–Al–Zn–Mn alloys were investigated in aqueous acidic, neutral and basic solutions. Conventional electrochemical techniques such as open-circuit potential measurements, polarization methods and electrochemical impedance spectroscopy (EIS) were used. The results have shown that the rate of corrosion in acidic solution is relatively high compared to that in neutral or basic solutions. The presence of Al, Zn and Mn as alloying elements decreases the rate of corrosion of the alloy. The activation energy of the corrosion process occurring at the surface of Mg or Mg alloys in aqueous solutions is less than 40 kJ mol^{-1}. This value indicates a one electron transfer electrode as a rate controlling process. The impedance data were fitted to equivalent circuit models that explain the different electrochemical processes occurring at the electrode/electrolyte interface.

1. Introduction

Magnesium alloys containing 2–10% Al with minor additions of Zn and Mn are widely used for different technological applications. These alloys are comparatively cheap and possess attractive characteristics, especially machinability and corrosion resistance at temperatures above 100 °C [1]. The alloys have high stiffness to weight ratio, ease of workability, high damping capacity, castability, weld-ability and recyclability [2]. Because of these excellent properties they are mostly used in aerospace and automotive industries. The alloy design development, surface treatment methods and understanding of corrosion mechanisms have extended the potential applications of the Mg alloys [3]. The corrosion resistance of the alloy depends on its composition, microstructure and ambient medium. It is sensitive to the chloride ion concentration and the pH of the environments [4,5]. In neutral and basic solutions the corrosion resistance is relatively high because of the formation of a partially protective $Mg(OH)_2$ layer on the alloy surface [4]. The presence of chloride ions promotes the dissolution of the protective layer and leads to increased rates of corrosion [4,6].

The corrosion of Mg alloys in non-oxidizing neutral or basic chloride solutions at free-corrosion potential initiates as irregular pits. The mechanism of the corrosion process is quite different from the auto-catalytic pitting experienced by stainless steels and the local increase of pH resulting from the formation of $Mg(OH)_2$ has no effect on the pitting process [7,8]. The film is not very stable and its free-corrosion potential is more positive than the pitting potential for both single α phase alloys as well as for two phase (α + β) alloys [9–11]. The corrosion of Mg is a localized corrosion, which starts at irregular pits that spread laterally and cover the whole surface [11,12]. In two phase Mg alloys the corrosion mechanism is influenced by microstructures. Fine, uniformly dispersed, cathodic phases are the most detrimental to the corrosion resistance of Mg-base alloys [13]. The casting method influences the corrosion performance through control of the microstructures [14]. The presence of alloying elements with Mg not only modifies its mechanical properties but also improves its corrosion resistance [15].

In this paper it is aimed at the investigation of the corrosion and passivation behaviors of Mg and two different Mg alloys in aqueous solutions covering the acidic, neutral and basic ranges. The effect of temperature on the corrosion rate and the determination of the molar activation energy of the corrosion process have been carried out. Equivalent circuit models for the electrode/electrolyte interface were suggested.

2. Experimental

The working electrodes were made from massive rods of Mg (99.9% + 0.03% Cu, 0.03% Ni and 0.04% Fe), Mg–Al–Zn (92% Mg + 7% Al and 1% Zn) and Mg–Al–Zn–Mn (89.2% Mg + 10% Al, 0.5% Zn and

* Corresponding author. Tel.: +20 2 35676558; fax: +20 2 35685799.
E-mail addresses: wbadawy50@hotmail.com, wbadawy@cu.edu.eg (W.A. Badawy).

0013-4686/$ – see front matter © 2009 Elsevier Ltd. All rights reserved.
doi:10.1016/j.electacta.2009.10.083

0.3% Mn). The metallic rods were mounted in suitable glass tubes by two component epoxy resin leaving a surface area of 0.50 cm^2 to contact the solution. The electrochemical cell was a three electrode all-glass cell with a Pt-counter and a saturated calomel reference (SCE) electrodes. Before each experiment the working electrode was mechanically polished using successive grades emery papers down to 2000 grit, rubbed against a smooth polishing cloth then washed with triple distilled water and transferred quickly to the electrolytic cell. The electrochemical measurements were carried out in aqueous solutions, where analytical grade reagents and triple distilled water were always used. The test electrolytes were buffer solutions of pH 2 (44.2 mL 0.1 M $COOKC_6H_4COOH$ + 54.3 mL 0.1 M HCl + 151.5 mL H_2O), pH 7 (113.6 mL 0.1 M KH_2PO_4 + 56.8 mL 0.1 M NaOH + 79.6 mL H_2O), and pH 12 (100 mL 0.2 M KH_2PO_4 + 163.7 mL 0.2 M NaOH).

Before each measurement, the pH of the test electrolyte was controlled by a standard pH-meter. The electrochemical measurements were performed using a Voltalab 10 PGZ 100 "All-in-one" potentiostat/galvanostat. The system is provided by an interruption unit to compensate any ohmic, (IR), drop between the working and the reference electrodes and the potentiodynamic polarization curves were extrapolated automatically to the most linear part of the Tafel lines. The impedance, Z, and the phase shift, θ, were measured in the frequency range 0.1–10^5 Hz. The superimposed ac-signal was 10 mV peak to peak amplitude. To achieve reproducibility, each experiment was carried out at least twice. All potentials were measured against and referred to the SCE at room temperature of 25 ± 1 °C. The potentiodynamic polarization experiments were carried out at a scan rate of 10 mV s^{-1}. Details of experimental procedures are as described elsewhere [16,17].

3. Results and discussion

3.1. Open-circuit potential measurements

The open-circuit potential (OCP) of the materials under investigation was followed over 180 min in naturally aerated aqueous solutions of pH 2, 7 and 12. The results of these experiments are presented in Fig. 1a–c for Mg, Mg–Al–Zn and Mg–Al–Zn–Mn in the three different electrolytes, respectively. The results show that Mg and its alloys tend to passivate in aqueous solutions. The open-circuit potential gets more positive and the steady state corrosion potential is achieved within 1 h from electrode immersion in the solution and the values are presented in Table 1. Longer times of immersion up to 6 h did not show significant effect on the steady state potential and did not affect the polarization experiments. The steady state potential of Mg is more positive than that of the two alloys (cf. Table 1).

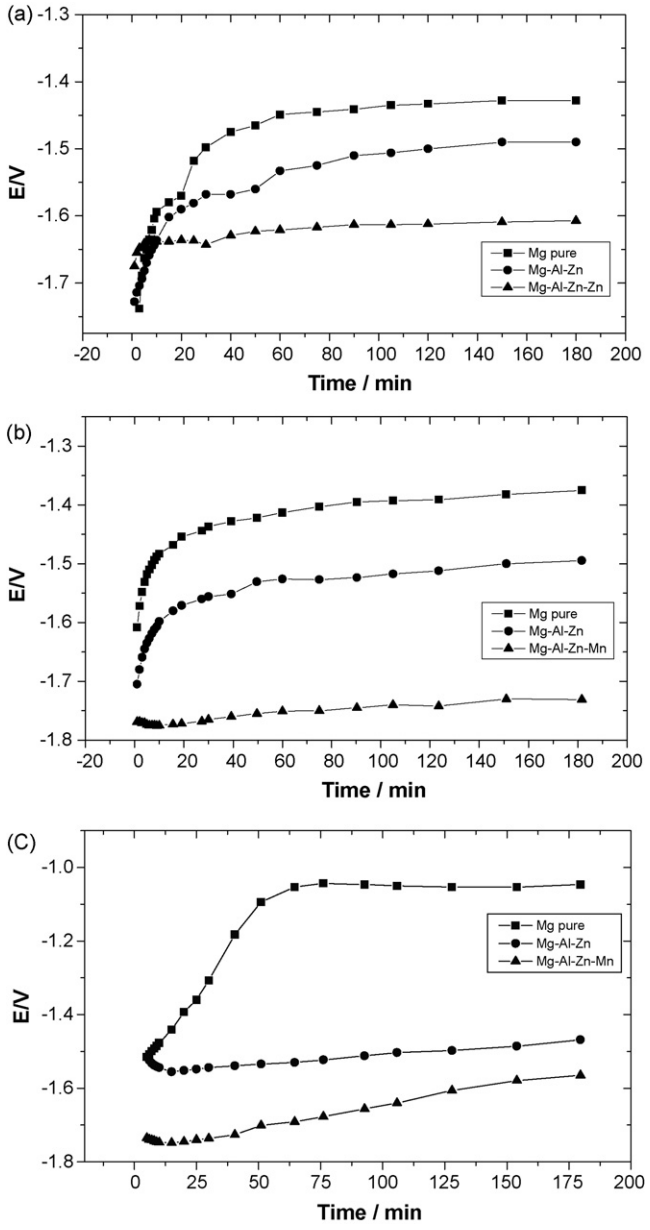

Fig. 1. Variation of the open-circuit potentials of Mg and the two alloys with time in naturally aerated aqueous solutions of different pH at 25 °C: (a) pH 2, (b) pH 7 and (c) pH 12.

3.2. Potentiodynamic polarization measurements

The potentiodynamic polarization curves of Mg and the two alloys are presented in Fig. 2a–c in solutions of pH 2, 7 and 12, respectively. The measurements were carried out after reaching the steady state (90 min after electrode immersion in the test solution) in naturally aerated solutions at a scan rate of 10 mV s^{-1}. In all solutions the tendency for corrosion occurs. The corrosion parameters, corrosion potential, E_{corr}, corrosion current density, i_{corr}, and corrosion resistance, R_{corr}, were calculated from the automatically extrapolated Tafel lines. The corrosion current density was used for the calculation of the corrosion rate in mm y^{-1} according to the Faraday's law [18]:

$$\text{Corrosion rate } (\text{mm y}^{-1}) = 3.27 \times 10^{-3} \times i_{corr}\ (\mu\text{A cm}^{-2}) \times \frac{\text{M}\,(\text{g mol}^{-1})}{n} \times d\ (\text{g cm}^{-3})$$

The factor 3.7×10^{-3} includes the Faraday's constant, and the metric and time conversion factors, d is the density, M the molecular mass and n the number of equivalents (number of exchanged electrons in the corrosion process). The calculated parameters for the three materials in the three different solutions are presented in Table 1. The results show apparent changes in the corrosion potential and corrosion current density values of Mg according to the alloying condition. In general, the shape of the polarization curves is almost the same and the presence of alloying elements does not make significant changes in the shape, which suggests a similar electrochemical behavior. The appearance of an anodic current plateau in the neutral and basic solutions suggests a pseudo-passivation step [19,20]. Fig. 3 presents the potentiodynamic polarization curves of the three investigated materials [Mg in Fig. 3a, Mg–Al–Zn in Fig. 3b and Mg–Al–Zn–Mn in Fig. 3c], separately, in the acidic, neutral and basic solutions. The results show the similarity of the curves and indicate that there is no passivity in

Table 1
Polarization parameters and rates of corrosion of Mg and the two alloys in naturally aerated solutions of pH 2,7 and 12 at 25 °C.

Sample	pH = 2				pH = 7				pH = 12			
	E_{corr}/V	i_{corr}/μA cm^{-2}	R_{corr}/ Ω cm^2	Rate/ mm y^{-1}	E_{corr}/V	i_{corr}/μA cm^{-2}	R_{corr}/ Ω cm^2	Rate/ mm y^{-1}	E_{corr}/V	i_{corr}/μA cm^{-2}	R_{corr}/ Ω cm^2	Rate/ mm y^{-1}
Mg	−1.458	230	88	5.25	−1.550	64.5	254	1.56	−1.426	5.1	4250	0.12
Mg–Al–Zn	−1.530	144	113	3.28	−1.668	44.5	410	1.01	−1.522	5.1	4260	0.12
Mg–Al–Zn–Mn	−1.628	89	130	2.04	−1.796	38.9	650	0.89	−1.658	2.9	5680	0.06

the acidic solutions. The corrosion current density of Mg in acidic solution is more than 3 times that recorded in neutral solutions and about 45 times that recorded in basic media. The same trend was also observed with the two alloys.

Although that the corrosion potential of the alloys is more negative than that of Mg, the rate of corrosion of the alloys is less than that of the metal itself, i.e. the presence of the alloying elements in the Mg matrix decreases the corrosion rate, in other words it leads to a significant increase in the corrosion resistance [21]. The relatively higher corrosion rate of Mg can be attributed to the pres-

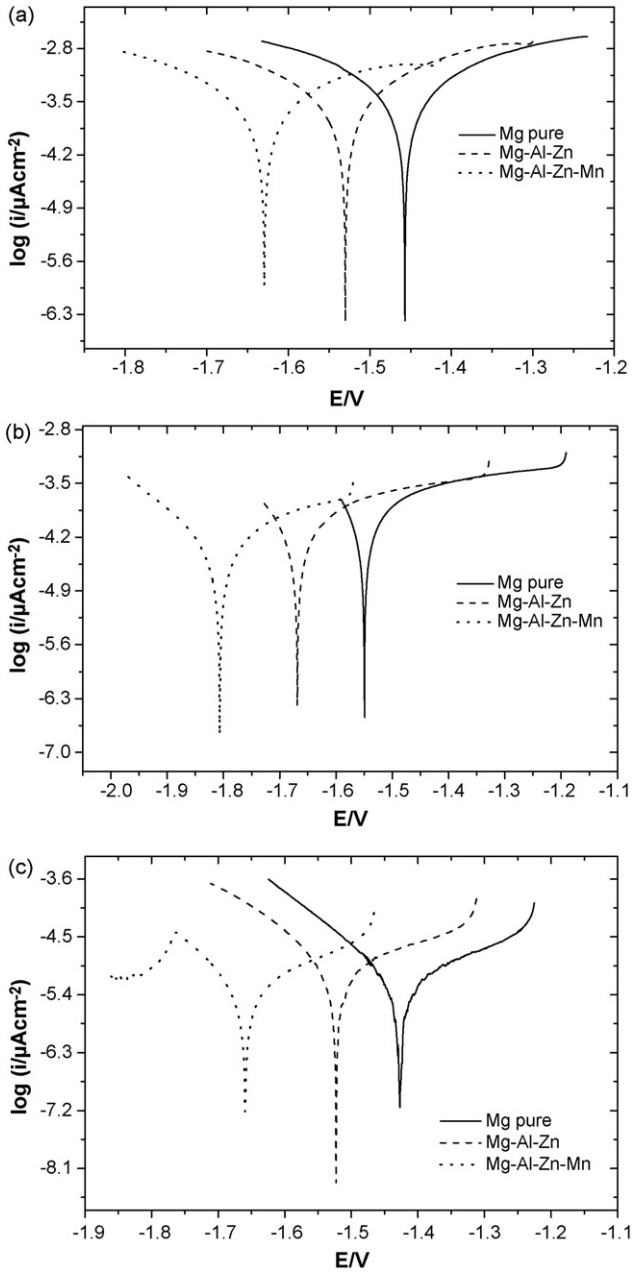

Fig. 2. Potentiodynamic polarization curves for Mg, Mg–Al–Zn and Mg–Al–Zn–Mn alloys in naturally aerated aqueous solutions of different pH at 25 °C: (a) pH 2, (b) pH 7 and (c) pH 12.

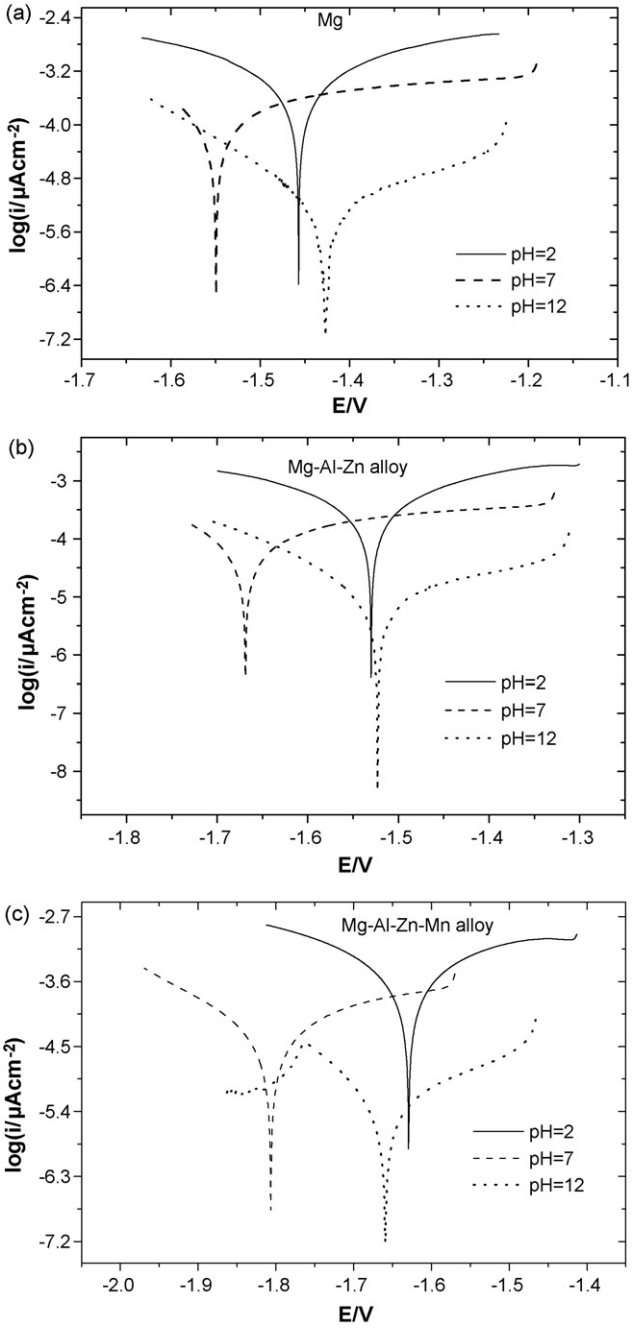

Fig. 3. Potentiodynamic polarization curves of the three different materials in naturally aerated aqueous solutions of different pH at 25 °C: (a) Mg, (b) Mg–Al–Zn and (c) Mg–Al–Zn–Mn.

Table 2
Activation energies of the corrosion of Mg and the two alloys in naturally aerated solution of pH 2, 7 and 12.

Sample	E_a/kJ mol^{-1}		
	pH = 2	pH = 7	pH = 12
Mg	8.0	9.9	10.3
Mg–Al–Zn	8.7	10.4	10.2
Mg–Al–Zn–Mn	8.6	11.3	14.7

ence of Fe impurity that exceeds the tolerance limit, which was reported to be 0.017% in Mg alloys [13]. Away from this impurity level and alloying elements and as it can be expected for active metals, the rate of corrosion of these metallic materials in acidic medium is relatively high compared to that in neutral or basic solutions. Also, no reproducible data could be obtained in acidic solutions. The calculated values of the corrosion rates of the three materials in the three different solutions are presented in Table 1. The calculated values, either from the polarization measurements or from the impedance data, show clearly that the three investigated materials have comparable corrosion rates in basic solutions. This can be explained by the formation of a barrier layer of $Mg(OH)_2$ which is insoluble in basic solutions [4,22]. In acidic solutions, no barrier layer can be formed, since $Mg(OH)_2$ is simultaneously soluble and hence higher corrosion rates were recorded. In neutral solutions, the barrier magnesium hydroxide layer is partially soluble and so a decrease in the rate of corrosion compared to the acid solution was recorded. From the three investigated materials, the Mg–Al–Zn–Mn alloy shows the lowest corrosion rate and Mg metal possesses the highest one. The low corrosion rate of the alloy is due to the presence of alloying elements, especially Mn. Small additions of Mn increases the corrosion resistance of the alloy and at the same time reduces the effects of metallic impurities [15,23].

3.3. Effect of temperature

The effect of temperature on the corrosion and passivation behaviors of Mg, Mg–Al–Zn and Mg–Al–Zn–Mn was investigated. An all-glass double-walled electrochemical cell with the same arrangements as described before was used. The measurements were performed in unstirred naturally aerated buffer solutions of pH 2, 7 and 12 in the temperature range between 285 and 315 K. In general, the rate of corrosion increases as the temperature increases. At each temperature, the corrosion current density, i_{corr}, was obtained from the polarization measurements. A plot of log i_{corr} versus $1/T$ was found to obey the familiar Arrhenius equation [24].

$$\frac{d\log i_{corr}}{d(1/T)} = \frac{-E_a}{R}$$

where E_a is the molar activation energy of the corrosion process and R is the gas constant (8.314 J mol^{-1} K^{-1}). The corresponding Arrhenius plots are presented in Fig. 4a–c for Mg, Mg–Al–Zn and Mg–Al–Zn–Mn in the three different solutions. The activation energy of the corrosion process was calculated from the slope of the corresponding Arrhenius plot. The calculated values for the different materials in the three solutions are presented in Table 2. The calculated activation energy values are <40 kJ mol^{-1}, which means that the rate determining step in the corrosion process is one electron transfer process [25,26].

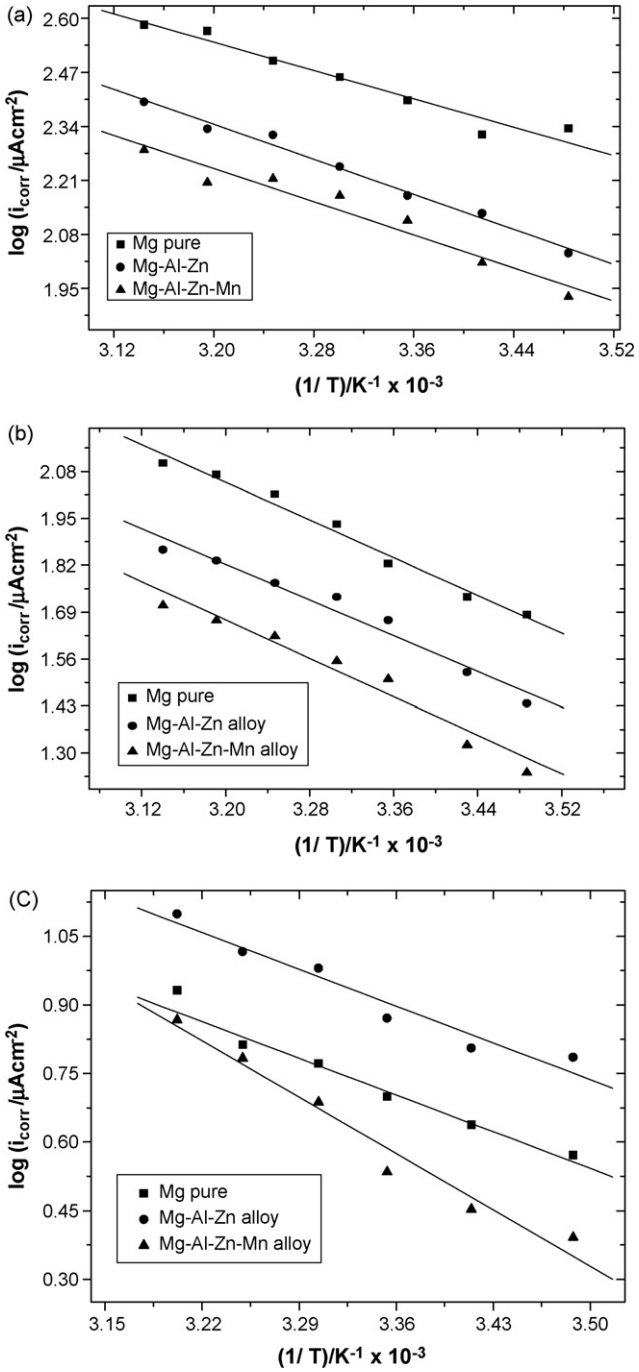

Fig. 4. Arrhenius Plots (log i_{corr} vs. $1/T$ relations) for the corrosion behavior of Mg, Mg–Al–Zn and Mg–Al–Zn–Mn alloys in naturally aerated solutions of different pH: (a) pH 2, (b) pH 7 and (c) pH 12.

3.4. The electrochemical impedance measurements

Electrochemical impedance spectroscopy (EIS) is essentially a steady state technique that is capable of accessing relaxation phenomena whose relaxation times vary over orders of magnitudes and permits single averaging within a single experiment to obtain high precision levels. It confirms the conventional polarization techniques for corrosion rate measurements. Open-circuit impedance of Mg and the two alloys was traced over 90 min from electrode immersion in the test solutions. Longer immersion of the electrodes in the electrolyte did not show reasonable changes. Some experiments were carried out after 6 h of the electrode

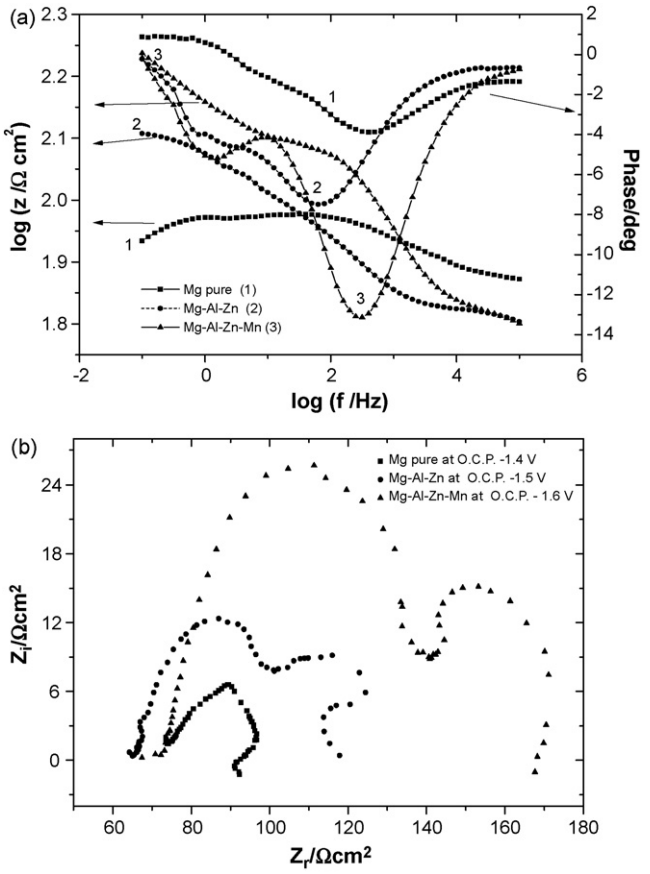

Fig. 5. Impedance plots for Mg, Mg–Al–Zn and Mg–Al–Zn–Mn alloys in naturally aerated solutions of pH 2 at 25 °C. [■, ▲, ● represent experimental data and continuous lines are fitted data.] (a) Bode plots and (b) Nyquist plots.

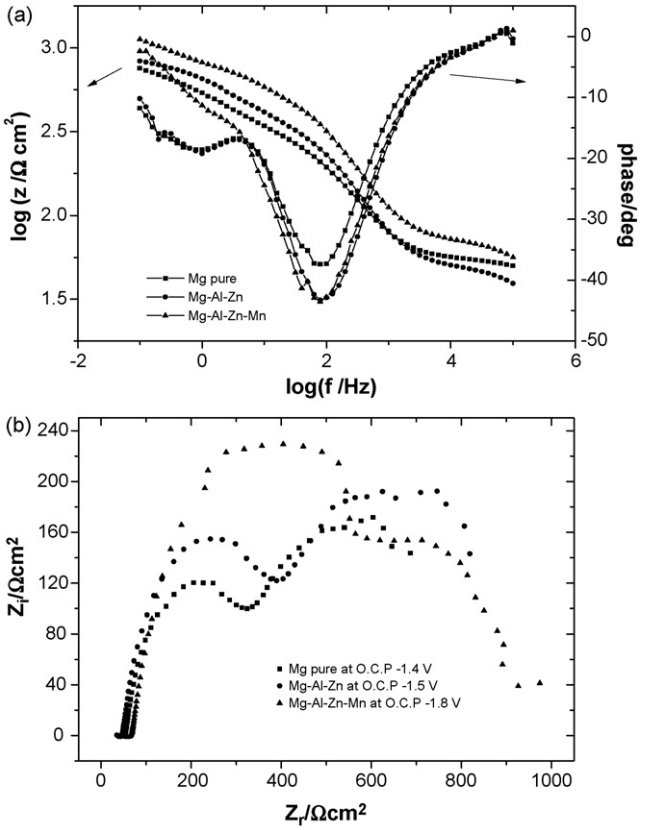

Fig. 6. Impedance plots for Mg, Mg–Al–Zn and Mg–Al–Zn–Mn alloys in naturally aerated solutions of pH 7 at 25 °C. [■, ▲, ● represent experimental data and continuous lines are fitted data.] (a) Bode plots and (b) Nyquist plots.

immersion in the different solutions. Typical data for the three materials in aqueous solutions of pH 2, 7 and 12 are presented as Bode and Nyquist plots in Figs. 5–7 in acidic, neutral and basic solutions, respectively. Bode plots are recommended as standard impedance plots, since the phase angle, θ, is a sensitive parameter for indicating the presence of additional time constants in the impedance spectra and the whole impedance data are presented explicitly. Nyquist plots are presenting a direct comparison of the corrosion resistance of the different materials in the various solutions. It gives also a direct indication of the presence of different rate controlling steps and also diffusion controlled processes [27–30].

In Fig. 5a Bode plots of Mg, Mg–Al–Zn and Mg–Al–Zn–Mn alloys in aqueous solution of pH 2 are presented. The figure shows two phase maxima at low and high frequencies for the three investigated materials which assigns the presence of two time constants controlling the corrosion process. The first at the law frequency region can be attributed to the charge transfer (corrosion) resistance, R_{ct}, and the double-layer capacitance, C_{dl}, at the electrode surface, while the second at high frequency is attributed to a partially protective surface film of $Mg(OH)_2$ [31–33]. The impedance spectra are similar except for the diameters of the loops assigning the corrosion resistance (cf. Nyquist plots). This similarity means that the corrosion mechanism of these materials is the same, but they possess different corrosion rates [34]. In order to enable an accurate analysis of the impedance data equivalent circuit models have been suggested (cf. Fig. 8). In the model presented in Fig. 8a, R_s represents the solution resistance, R_{ct} the charge transfer (corrosion) resistance, i.e. the resistance to the electron transfer of the faradic process on the metal surface, in parallel to a capacitor representing the double-layer capacity, C_{dl}. To account for the capacitance and resistance of the surface film formed on the electrode, an additional capacitor, C_f, and a resistance, R_f, were introduced. This model fits the impedance data obtained in acidic and neutral solutions. In basic solutions, where a clear diffusion controlled step was recorded (cf. Fig. 8b), the Warburg impedance, Z_w, was introduced to account for the diffusion process. It is worth to mention that both the charge transfer resistance, R_{ct}, and the barrier film resistance, R_f, represent the polarization resistance of the Tafel interpretation or the corrosion resistance that could be obtained from the corrosion measurements.

It was observed that the addition of alloying elements to Mg has led to an increase in the value of the absolute impedance, Z, which means that the presence of Al, Zn and Mn in the Mg matrix increases the corrosion resistance of the metallic material as can be seen in Figs. 6a and 7a.

In neutral solutions, compared to the acidic solutions, the phase maximum in the low frequency region is suppressed and that in the high frequency region dominates. This means that the corrosion rate of Mg and its alloys is decreased by the increase of the solution pH. The increase of the corrosion resistance of the alloy is due to the stability of the corrosion product formed as a protective film on the metallic surface at higher pH's. The protective film thus formed is relatively stable in neutral solutions but soluble in acid solutions [4].

The EIS spectra of Mg and the two alloys in basic solutions show only one phase maximum. The disappearance of the other phase maximum at the low frequency region and the relatively high impedance values recorded in basic solutions are good indication for the presence of a stable protective layer on the metallic surface. The results indicate that the corrosion process is controlled by the protective film formation and a diffusion controlled step.

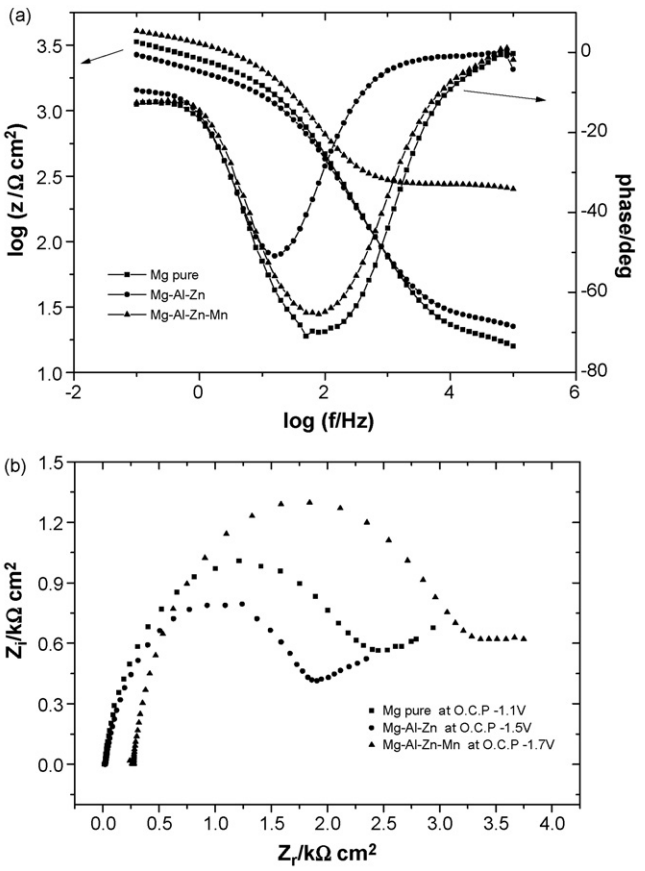

Fig. 7. Impedance plots for Mg, Mg–Al–Zn and Mg–Al–Zn–Mn alloys in naturally aerated solutions of pH 12 at 25 °C. [■, ▲, ● represent experimental data and continuous lines are fitted data.] (a) Bode plots and (b) Nyquist plots.

The impedance data for the three investigated materials after 90 min immersion in the aqueous solutions of pH 2, 7 and 12 were fitted to theoretical data according to the proposed model presented in Fig. 8 and the values of the impedance parameters were calculated and presented in Table 3. The values of the film resistance, R_f, are increasing with the increase of the pH of the solution. Also, the presence of the alloying elements improves the film resistance. The film resistance follows the order Mg < Mg–Al–Zn < Mg–Al–Zn–Mn at the same pH. These results are consistent with the results of the polarization measurements.

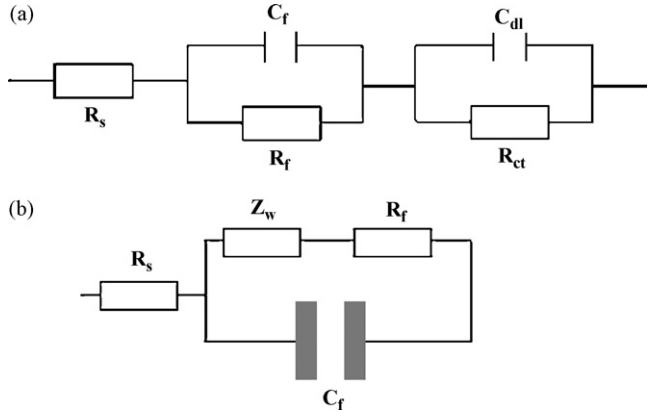

Fig. 8. Equivalent circuit models for fitting of the impedance data of Mg and its alloys, R_s = solution resistance, R_{ct} = charge transfer (corrosion) resistance, C_{dl} = electrode capacitance, R_f = film resistance, C_f = film capacitance and Z_w is the Warburg impedance. (a) Model for fitting the data in acidic and neutral solutions. (b) Model for fitting the data in basic solutions, where a Z_w was introduced to account for the diffusion controlled process.

Table 3
Equivalent circuit parameters for Mg and the two alloys in naturally aerated solutions of pH 2,7 and 12 at 25 °C.

pH	Sample	R_s/Ω cm²	R_f/Ω cm²	C_f/μf cm⁻²	R_{ct}/Ω cm²	C_{dl}/mf cm⁻²
2	Mg pure	72.5	20.5	12.2	5.4	2.4
	Mg–Al–Zn	64.8	44.2	72.0	30.1	6.7
	Mg–Al–Zn–Mn	73.4	70.6	11.3	34.5	5.8
7	Mg pure	53.0	340.5	23.4	578.6	994.9
	Mg–Al–Zn	47.0	425.2	18.7	498.7	797.7
	Mg–Al–Zn–Mn	68.8	613.9	13.0	579.5	137.3
12	Mg pure	12.7	2615	15.2		
	Mg–Al–Zn	23.8	2010	15.8		
	Mg–Al–Zn–Mn	266.7	3186	12.5		

From the above presented data, it can be concluded that Mg either pure or in the alloy is the most active element and oxidized to oxide, hydroxide or the divalent ion in aqueous environments depending on the pH of the solution. The active sites at the metal are easily oxidized and separated from the electrode surface according

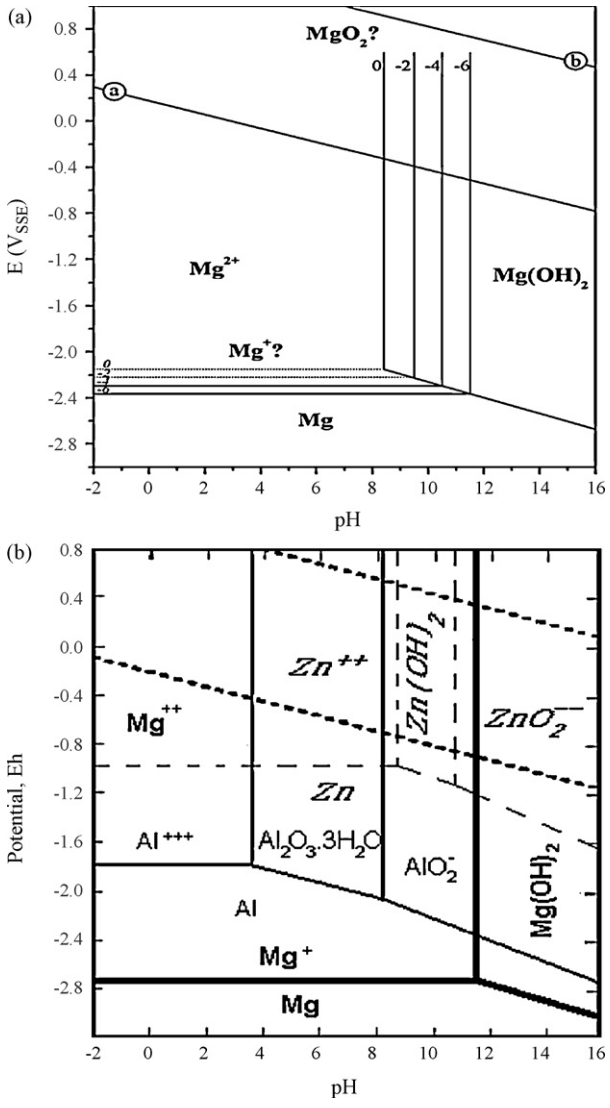

Fig. 9. Potential-pH diagrams of Mg (a), and Mg, Al, Zn (b).

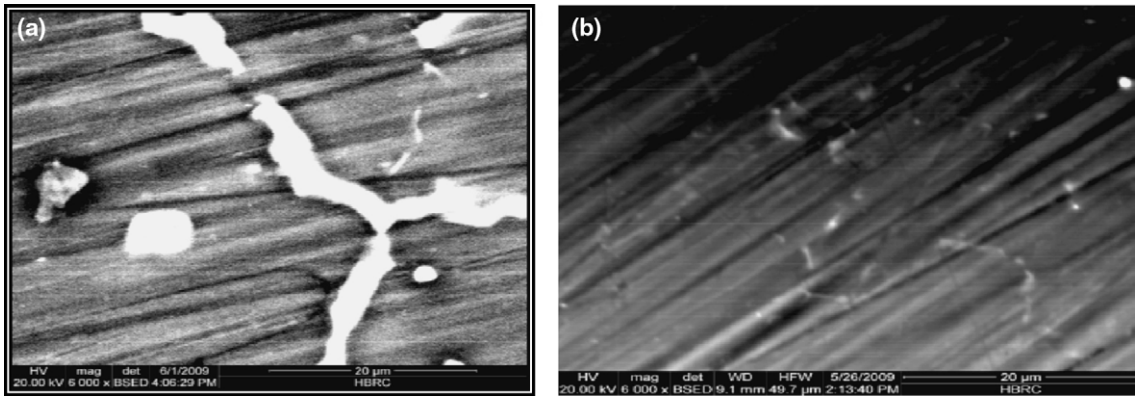

Fig. 10. Scanning electron micrographs of mechanically polished Mg–Al–Zn (a) and Mg–Al–Zn–Mn (b) alloys.

to [35]:

$$Mg \rightarrow Mg^{+} + e^{-}$$

which is consistent with a one electron transfer kinetics and the low activation energy of the corrosion process [23,26,36]. The monovalent ion is further oxidized by the H^{+} ions in acid solutions as

$$2Mg^{+} + 2H^{+} \rightarrow 2Mg^{2+} + H_2$$

or, by water molecules in neutral solutions under the formation of $Mg(OH)_2$ as corrosion product [14,21]:

$$2Mg^{+} + 2H_2O \rightarrow 2Mg^{2+} + 2OH^{-} + H_2$$

$$Mg^{2+} + 2OH^{-} \rightarrow Mg(OH)_2 \qquad \text{(corrosion product)}$$

The formation of the stable magnesium hydroxide as protective layer on the metallic surface is responsible for the relatively high impedance and corrosion resistance of the materials in neutral or alkaline solutions. It is also possible that a disproportionation reaction of the Mg^{+} ions into magnesium metal and Mg^{2+} ions may take place according to:

$$2Mg^{+} \rightarrow Mg + Mg^{2+}$$

The magnesium atoms thus formed represent active centers that can be oxidized in neutral or basic solutions to give a stable corrosion product according to:

$$Mg + 2H_2O \rightarrow Mg(OH)_2 + H_2$$

The recorded effect of pH on the corrosion and passivation behavior of Mg and its alloys is consistent with the potential-pH diagrams of these materials presented in Fig. 9a for Mg and Fig. 9b for Mg, Al and Zn [37,38]. According to these diagrams the dissolution of Mg in aqueous solutions proceeds via reduction of water and the formation of $Mg(OH)_2$ which is soluble in acidic solutions leading to the recorded high corrosion rate. At pH ≥ 4, this corrosion product is stable and hence lower corrosion rates can be measured. In the pH range 4–9, $Mg(OH)_2$ is stable and Al is passive and above pH 9 the formation of magnesium aluminates and stabilization of $Mg(OH)_2$ occurs. In the range between 8.5 and 10.5 Zn is also passive. The formation of microstructures due to the presence of alloying elements in some Mg alloys leads to the stabilization of the alloy and higher corrosion resistance values were recorded [6,20,34,39]. For example, the as-cast microstructures of Mg–9Al–1Zn (AZ91) alloy consist mainly of α-Mg matrix and β-$Mg_{17}Al_{12}$ intermetallic. This intermetallic is more stable than the α-Mg matrix because of its high Al content. The β-$Mg_{17}Al_{12}$ phase acts as an effective barrier and as an active cathode for the α-Mg matrix. The oxide film on this intermetallic is continuous and inhibits the dissolution of the α-Mg phase [6]. The effect of alloying elements on the microstructure formation and the contribution of these elements to the improvement of the corrosion resistance of the alloys was clearly seen on the scanning electron micrographs presented in Figs. 10 and 11. In Fig. 10(a), the SEM of Mg–Al–Zn shows clearly the primary α-phase (Mg matrix) and large areas of β-phase ($Mg_{17}Al_{12}$) intermetallic. The large areas of this phase leads to the recorded relatively higher corrosion rates as indicated by the formation of the cylindrical deep pits present in the

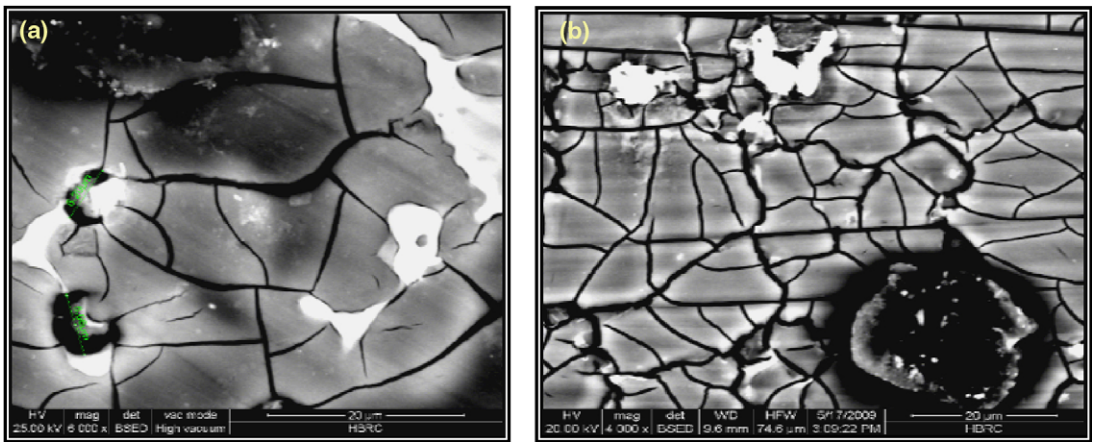

Fig. 11. Scanning electron micrographs of Mg–Al–Zn (a) and Mg–Al–Zn–Mn (b) alloys after 90 min immersion in naturally aerated solutions of pH 7 at 25 °C.

micrograph taken after 90 min immersion in the solution presented in Fig. 11a. In the Mg–Al–Zn–Mn alloy the areas of the intermetallic are decreased and seem that the surface does not contain such galvanic initiated corrosion process (cf. the micrograph of Fig. 10b). The corrosion of this alloy after immersion in the aqueous electrolyte is still present in the form of spots. Small cylindrical pits that have a diameter of approximately 6.2–6.7 μm are present. There are some flawed regions in the form of line cracks concentrated on the black α-phase which could be attributed to defaults on the oxide film (cf. the micrograph of Fig. 11b). It is worth to mention that Mg itself did not show structures that should be interpreted. It is more likely in the form of overall corrosion that is then suppressed by the formation of the passive $Mg(OH)_2$ as a stable corrosion product.

The improvement of the corrosion behavior of Mg alloys due to the alloying elements was reported to be due to: (i) refining of the β-phase and formation of more continuous network, or (ii) suppression of β-phase formation by forming another intermetallic, which is less harmful to the α-Mg matrix, which is clearly seen in the presented micrographs, and (iii) added elements may incorporate into the protective film and thus increasing its stability [40–42].

4. Conclusions

1. The corrosion rates of Mg, Mg–Al–Zn and Mg–Al–Zn–Mn alloys in acidic solution are three times that occurs in neutral solutions and more than 28 times that measured in basic solutions.
2. Addition of Al, Zn and Mn to Mg decreases the rate of corrosion of the metal and the Mg–Al–Zn–Mn was found to be the most corrosion resistant alloy.
3. The activation energy of the corrosion process is $<40\,kJ\,mol^{-1}$. This supports one electron transfer step as the rate determining corrosion process.
4. The EIS results have shown that the corrosion process involves a diffusion controlled step which is not occurring in acidic or neutral solutions.
5. The relatively high corrosion resistance in basic solutions is due to the formation of the stable $Mg(OH)_2$ barrier film on the metal surface.
6. SEM results have shown that the effect of the intermetallic β-phase ($Mg_{17}Al_{12}$) is suppressed or at least minimized in the presence of Zn and Mn.

References

[1] B.L. Mordike, T. Ebert, Mater. Sci. Eng. A 302 (2001) 37.
[2] E. Ghali, Magnesium and magnesium alloys, in: R.W. Revie (Ed.), Uhlig's Corrosion Handbook, John Wiley & Sons, New York, 2000, p. 793.
[3] D. Eliezer, E. Aghion, F.H. Froes, Adv. Perform. Mater. 5 (1998) 201.
[4] W.S. Loose, in: L.M. Pidgeon, J.C. Mathes, N.E. Woldmen (Eds.), Corrosion and Protection of Magnesium, ASM International, Materials Park, OH, 1946, p. 173.
[5] R. Ambat, N.N. Aung, W. Zhou, J. Appl. Electrochem. 30 (2000) 865.
[6] R. Ambat, N.N. Aung, W. Zhou, Corros. Sci. 42 (2000) 1433.
[7] R. Tunold, H. Holtan, M.-B.H. Berge, A. Lasson, R. Steen-Hansen, Corros. Sci. 17 (1977) 353.
[8] G. Song, A. Atrens, Adv. Eng. Mater. 9 (2007) 177.
[9] A. Atrens, R. Coade, J. Allison, H. Kohl, G. Hochoertler, G. Krist, Mater. Sci. Forum 17 (1993) 263.
[10] G. Song, A. Atrens, D. St John, J. Nairn, Y. Lang, Corros. Sci. 39 (1997) 855.
[11] G. Song, A. Atrens, Adv. Eng. Mater. 5 (2003) 837.
[12] G. Song, A. Atrens, D. St John, X. Wu, J. Nairn, Corros. Sci. 39 (1997) 1981.
[13] G.L. Marker, J. Kruger, K. Sieradzki, J. Electrochem. Soc. 139 (1992) 47.
[14] G. Song, A. Atrens, Dargusch, Corros. Sci. 41 (1999) 249.
[15] B.E. Carlson, J.W. Jones, The metallurgical aspects of the corrosion behavior of cast Mg–Al alloys, in: Light Metals Processing and Applications, METSOC Conference, Quebec, 1993.
[16] R.M. El-Sherif, K.M. Ismail, W.A. Badawy, Electrochim. Acta 49 (2004) 5139.
[17] W.A. Badawy, K.M. Ismail, A.M. Fathi, J. Appl. Electrochem. 35 (2004) 879.
[18] S.W. Dean, Handbook on Corrosion Testing and Evaluation, John Wiley & Sons, New York, 1971, p. 171.
[19] P.L. Bonora, M. Andrei, A. Eliezer, E.M. Gutman, Corros. Sci. 44 (2002) 729.
[20] Y. Song, D. Shan, R. Chen, En.-H. Han, Corros. Sci. 51 (2009) 1087.
[21] G. Song, A. Atrens, Adv. Eng. Mater. 1 (1999) 11.
[22] G. Song, A. Atrens, X. Wu, B. Zhang, Corros. Sci. 40 (1998) 1769.
[23] I.J. Polmer, Physical Metallurgy of Magnesium alloys, DGM Informationsgesellschaft, Oberursel, Germany, 1992, p. 201.
[24] Martimer RG, Physical Chemistry, The Benjamin/Cummings Publishing Company, Inc., Redwood City, CA, 1983, p. 822.
[25] A. Wieckowski, E. Ghali, Electrochim. Acta 30 (1985) 1423.
[26] F.M. Al-Kharafi, W.A. Badawy, Corrosion 54 (1998) 377.
[27] A.J. Brock, G.C. Wood, Electrochim. Acta 12 (1967) 395.
[28] D.D. Macdonald, S. Real, S.I. Smedley, M. Uraquidi-Macdonald, J. Electrochem. Soc. 135 (1988) 2410.
[29] C.M.A. Brett, Corros. Sci. 33 (1992) 203.
[30] W.A. Badawy, K.M. Ismail, Electrochim. Acta 38 (1993) 2231.
[31] F. Rosalbino, E. Angelini, S. De Negri, A. Saccone, S. Delfino, Intermetallics 13 (2005) 55.
[32] F. Rosalbino, E. Angelini, S. De Negri, A. Saccone, S. Delfino, Intermetallics 14 (2006) 1487.
[33] Z. Xuehua, H. Yuanwei, W. Zhongling, C. Qiurong, G. Fuxing, Corros. Sci. 48 (2006) 4223.
[34] G. Song, A.L. Bowles, D.H. St John, Mater. Sci. Eng. A 366 (2004) 74.
[35] A.J. Bard, Encyclopedia of Electrochemistry of the Elements, vol. VIII, Marcel Dekker, New York, 1978.
[36] G.A. Wright, J. Electrochem. Soc. 114 (1967) 1263.
[37] M. Pourbaix, Atlas of Electrochemical Equilibrium Diagrams in Aqueous Solutions, NACE, Houston, TX, 1966.
[38] G.G. Perrault, Electroanal. Chem. Interface Electrochem. 51 (1974) 107.
[39] S. Mathieu, C. Rapin, J. Steinmetz, P.A. Steinmetz, Corros. Sci. 45 (2003) 2741.
[40] W. Guohua, F. Yu, G. Hongtao, Z. Chunquan, Z.Y. Ping, Mater. Sci. Eng. A 408 (2005) 255.
[41] F. Yu, W. Guohua, Z. Chunquan, Mater. Sci. Eng. A 433 (2006) 208.
[42] F. Yu, W. Guohua, G. Hongtao, L. Guanqun, Z. Chunquan, J. Mater. Sci. 41 (2006) 5409.